J. Fluid Mech. (1995), *vol.* 286, *pp.* 49–65

The effects of laterally sloping upper and lower boundaries on waves and instability in stratified shear flows

By S. A. THORPE AND J. T. HOLT
Department of Oceanography, The University, Southampton SO9 5NH, UK

(Received 8 March 1994 and in revised form 14 June 1994)

The dispersion relation for internal waves travelling in the horizontal direction of a two-dimensional stratified shear flow is affected by the presence of topography, or upper and lower boundaries, which vary only in the horizontal direction normal to that of the flow. This is in accordance with Grimshaw's (1978) findings for long internal waves. Such topography, however, imposes boundary conditions which affect both the growth rates and orientation of the crests of unstable disturbances. Predictions are derived for the particular case of instability of a fluid with a thin interface separating two fluids of different densities in relative flow, which are confined in a tube with horizontal generators but which has upper and lower parallel plane boundaries inclined to the horizontal at an angle α. These predictions are compared with laboratory experiments. There is good qualitative agreement and some quantitative agreement, at least when the predicted angle, γ, between the crest lines of the disturbances and the cross-flow direction, is small. Relatively small disturbances, or billow, amplitudes are found along the centreline of the tube. At large γ, however, the disturbance crests becomes less well-ordered, with billows on one side of the tube centreline connecting with neighbouring pairs on the other, so evolving a zigzag pattern. The results have application to naturally occurring flows in estuaries and channels, and to the development of instability in the stratified atmosphere.

1. Introduction

Both freely propagating waves and the development of instability, occurring in the stably stratified shear flows which occur in the natural fluid environment, will be affected by the presence of the underlying topography, for example by ridges and valley slopes in the atmosphere, by oceanic continental slopes or the cross-sectional shape of estuaries and sea straits, and the slopes of the boundaries of lakes. We have chosen for simplicity to study the effect of topography which varies in a direction transverse to the mean flow, as it might for flow in a channel of uniform cross-section or flow parallel to the contours of a slope, so that the mean motion may be taken to be horizontally uniform, unchanging with distance along the sloping boundary, but possibly changing with height.

The propagation of long interfacial waves in a stratified fluid in a non-rotating channel of arbitrary cross-section has been studied by Grimshaw (1978), who concluded that the phase of the waves is independent of the cross-channel y-coordinate, so that wave crests are everywhere normal to the down-channel x-direction in which the waves advance. 'Billows' developing in a stratified shear flow in rectangular channel with horizontal boundaries are also observed to be orientated, on

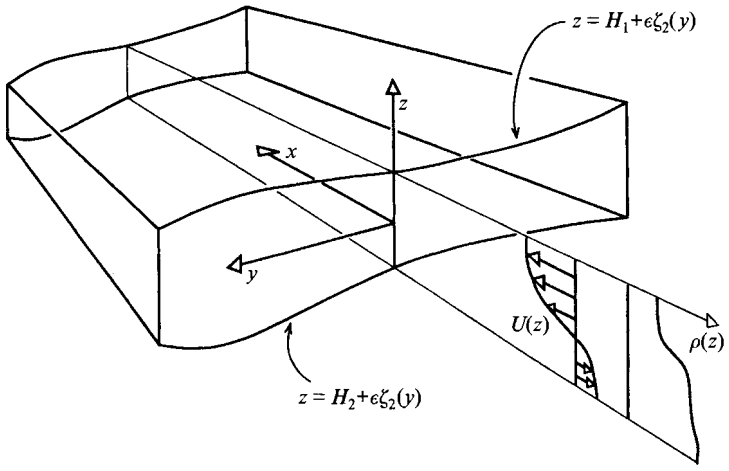

FIGURE 1. The coordinate system.

average, normal to the (vertical) sidewalls, that is with constant phase lines normal to the flow or in the direction of the mean flow vorticity vector (Thorpe 1971). This is consistent with Yih's (1955) extension of Squire's theorem, although the theorem places no limitation on the development of instability imposed by the presence of boundaries.

We show here that, whilst the crests of internal waves propagating along topography in non-rotating stratified shear flow have generally no phase shift, unstable disturbances or 'billows' may be tilted across the flow by the presence of topography. The effect is demonstrated both analytically (§2) and by laboratory experiments (§3).

2. Theory

2.1. *The general solution*

We consider small displacements in an inviscid non-diffusive stably stratified shear flow parallel to the horizontal x-direction. The fluid density, $\rho(z)$, and velocity, $(U(z), 0, 0)$, vary only in the vertical z-direction, and the fluid is confined between fixed upper and lower boundaries, the level of which varies in the second horizontal direction, y, normal to x and z, and transverse to the flow, as shown in figure 1. Infinitesimal disturbances are governed by the equation

$$\frac{\partial^2 w}{\partial z^2} + \left[\left(\frac{N^2}{(U-c)^2} - k^2\right)\left(1 - k^{-2}\frac{\partial^2}{\partial y^2}\right) - \frac{U''}{(U-c)}\right] w = 0, \tag{1}$$

where $w^* = w(y,z)\exp ik(x-ct)$ is the vertical velocity, k is the (real) x-wavenumber component of the disturbance, c is the phase speed, which may be complex, N is the buoyancy frequency, and $U'' = \mathrm{d}^2U/\mathrm{d}z^2$. The Boussinesq approximation has been made in deriving (1). When there is no variation in the y-direction, (1) reduces to the Taylor–Goldstein equation (Drazin & Reid 1981). The corresponding x- and y-components of the perturbation velocity, u^* and v^* respectively, are related to w by

$$k(U-c)\left[\frac{\partial^2}{\partial y^2} - k^2\right] u = \mathrm{i}\left[U'\frac{\partial^2}{\partial y^2} - k^2(U-c)\frac{\partial}{\partial z}\right] w \tag{2}$$

and

$$k^2(U-c)v = -\mathrm{i}k(U-c)\frac{\partial u}{\partial y} - U'\frac{\partial w}{\partial y}, \tag{3}$$

where $(u^*, v^*) = (u, v)\exp ik(x-ct)$ and $U' = \mathrm{d}U/\mathrm{d}z$. The boundary conditions are

$$w^* = \epsilon v^* \frac{\mathrm{d}\zeta_i}{\mathrm{d}y} \quad \text{at} \quad z = H_i + \epsilon\zeta_i(y), \quad i = 1, 2, \tag{4}$$

where we have introduced an ordering parameter, ϵ (which may subsequently be equated to unity), and we shall assume that $\epsilon\zeta_i \ll H_i$ and, in particular, that $\epsilon\,\mathrm{d}\zeta_i/\mathrm{d}y$ is small. We shall assume that the ζ_i can be expressed as Fourier series in y with periodicity selected so that $v = 0$ at positions, or at lateral boundaries, where $y = \pm b$, and that solutions for a general boundary shape can be found by superimposing solutions which separately satisfy each Fourier component. This will be further elaborated in §2.4. To illustrate the method, we select a component $\zeta_i = A_i \sin ly$. Paying regard to the appropriate phase relations imposed by the boundary conditions, we take

$$\left.\begin{aligned} u &= \delta[u_0 + \epsilon u_1 \sin ly + \epsilon^2(u_{21} + u_{22}\cos 2ly) + \ldots], \\ v &= \delta[\epsilon v_1 \cos ly + \epsilon^2 v_{22} \sin 2ly + \ldots], \\ w &= \delta[w_0 + \epsilon w_1 \sin ly + \epsilon^2(w_{21} + w_{22}\cos 2ly) + \ldots] \end{aligned}\right\} \tag{5}$$

and

$$c = c_0 + \epsilon c_1 + \epsilon^2 c_2 + O(\epsilon^3),$$

making a 'small transverse slope' perturbation, ϵ, to already small-amplitude waves. Here δ is an ordering parameter proportional to the disturbance amplitude at some given time. Higher-order terms in δ are neglected since (1)–(3) are already linearized in δ. The terms u_1, v_1, w_1, u_{12}, etc. are functions of z only. The boundary conditions (4) are expanded as Taylor series about $z = H_i$, and solutions are found by successive comparison of terms.

At order $\delta\epsilon^0$, (1) reduces to the Taylor–Goldstein equation with $c = c_0$, subject to the boundary condition $w_0 = 0$ at $z = H_i$ obtained from (4), providing an eigenvalue equation for c_0. Equation (2) gives $u_0 = (\mathrm{i}/k)\,\mathrm{d}w_0/\mathrm{d}z$, whilst (3) is satisfied identically.

At order $\delta\epsilon^1$, w_1 must satisfy

$$\mathscr{L}(k, l)\, w_1 \equiv \left\{\frac{\mathrm{d}^2}{\mathrm{d}z^2} + \left(\frac{N^2}{(U-c_0)^2} - k^2\right)\left(1 + \frac{l^2}{k^2}\right) - \frac{U''}{(U-c_0)}\right\} w_1 = 0, \tag{6}$$

with $c_1 = 0$ and the boundary conditions $w_1 = -A_i\,\mathrm{d}w_0/\mathrm{d}z$ at $z = H_i$. Equations (2) and (3) then give expressions for u_1 and v_1.

At order $\delta\epsilon^2$ we find that

$$\mathscr{L}(k, 0)\, w_{21} = c_2 \left\{\frac{U''(U-c_0) - 2N^2}{(U-c_0)^3}\right\} w_0, \tag{7}$$

with

$$w_{21} = \frac{A_i}{2(k^2+l^2)}\left\{\frac{A_i l^2 U'}{(U-c_0)}\frac{\mathrm{d}w_0}{\mathrm{d}z} - k^2\frac{\mathrm{d}w_1}{\mathrm{d}z}\right\} \quad \text{at} \quad z = H_i, \tag{8}$$

which provides an eigenvalue equation for c_2. We find also that

$$\mathscr{L}(k, 2l)\, w_{22} = 0, \tag{9}$$

with

$$w_{22} = \frac{A_i}{2(k^2+l^2)}\left\{\frac{A_i l^2 U'}{(U-c_0)}\frac{\mathrm{d}w_0}{\mathrm{d}z} + (k^2+2l^2)\frac{\mathrm{d}w_1}{\mathrm{d}z}\right\} \quad \text{at} \quad z = H_i. \tag{10}$$

The solution for the vertical component of the disturbance is

$$w^* = \delta[w_0 + \epsilon w_1 \sin ly + \epsilon^2(w_{12} + w_{22}\cos 2ly)]\exp\{ik[x - (c_0 + \epsilon^2 c_2)\,t]\}. \tag{11}$$

The displacement of an isopycnal surface $\rho(z_1)$ from the level $z = z_1$, say, is given (to the same order as terms in (11)) by $\eta^* = -\mathrm{i}w^*/[k(U-c)]$, evaluated at $z = z_1$ (Thorpe

1978). The solution, (11), represents a disturbance with amplitude modulated in the y-direction and with phase speed, $\mathrm{Re}\,(c_0+\epsilon^2 c_2)$, and growth rate $\mathrm{Im}\,\{k(c_0+\epsilon^2 c_2)\}$. If w_1 or w_{22} have imaginary parts, as (from (6) and (9)) will generally be the case if c_0 has an imaginary part, corresponding to unstable modes, then the disturbance will have a phase which varies in the y-direction:

$$w^* = W(y)\exp[\pm \mathrm{Im}\,(c_0+\epsilon^2 c_2)\,t]\exp\{\mathrm{i}[k\{x-\mathrm{Re}\,(c_0+\epsilon^2 c_2)\,t\}+\Phi(y)]\},$$

where $W(y)$ is the modulus and $\Phi(y)$ is the phase of the coefficient of the exponential term in (11). If however, w_1 and w_{22} are real, as is the case when c_0 lies outside the range of U and non-singular solutions of the Taylor–Goldstein equation represent shear-modified internal gravity waves (Banks, Drazin & Zaturska 1976), then $\Phi(y)$ will be zero and no shift of the wave phase with y will occur. Further, if the imaginary part of c_0 is zero, so that to first order the solutions represent stable solutions, then the imaginary part of c_2 is also zero. The stability boundary of the unstable disturbances is therefore not affected by the presence of boundaries, although as we shall find later (in §2.4), the growth rates of unstable modes may be reduced.

We now offer two examples in which analytical solutions can readily be found, before, in §2.4, deriving numerical results for a flow which can be realized in the laboratory.

2.2. *The case $U = 0$, $N =$ constant*

We seek the effects of sinusoidal topography on internal waves propagating in a fluid with no mean flow and uniform buoyancy frequency. Without loss of generality, we take $H_1 = -H_2 = H$ and, for illustration, we take $A_1 = A_2 = A$, so that the fluid is confined between boundaries at $\pm H + \epsilon A \sin ly$. We select the first-mode solution of the Taylor–Goldstein equation with $U = 0$,

$$w_0 = W\cos(\pi z/2H), \tag{12}$$

with $c_0^2 = N^2/[k^2+(\pi/2H)^2]$ and $u_0 = -(\mathrm{i}\pi/2kH)\,W\sin(\pi z/2H)$. At order $\delta\epsilon$,

$$w_1 = B\sin qz, \tag{13}$$

with $q = (\pi/2H)(1+l^2/k^2)^{1/2}$ and $B = (A\pi/2H)/\sin[(1+l^2/k^2)^{1/2}\pi/2]$, whilst at order $\delta\epsilon^2$

$$w_{21} = \frac{AB\pi^2}{2q(2kH)^2}\frac{\cos qH}{\cos q_1 H}\cos q_1 z, \tag{14}$$

$$w_{22} = Qc_2 z\sin\pi z/2H, \tag{15}$$

and

$$\frac{c_2}{c_0} = -\frac{A^2k^2(1+2l^2/k^2)(\pi/2kH)^4\cot qH}{[1+(\pi/2kH)^2]\pi(1+l^2/k^2)^{1/2}}, \tag{16}$$

with $Q = (2kH/\pi c_0)[k^2+(\pi/2H)^2]\,W$ and $q_1 = (\pi/2H)(1+4l^2/k^2)^{1/2}$. The terms w_1 and w_{22} are, as expected, real, so that the wave has no phase change in the y-direction. The phase speed c_2 is real and negative, implying that the effect of the sinusoidal topography is to reduce the phase speed. These results are consistent with those of Grimshaw (1978) for long internal waves.

2.3. *Two-layer shear flow*

A simple illustration of the effects of tilted boundaries on stable and unstable shear flows is given by a fluid with speed and density $(U,\rho) = (U_1,\rho_1)$ for $z > 0$, and $(U_2,\rho_2 > \rho_1)$ for $z < 0$, confined between rigid boundaries at $z = H_1 + A_1\sin ly$ and $z = -H_2 + A_2\sin ly$. We make the usual assumption that the flow in each layer is irrotational so that velocity potentials

$$\phi_i^* = \delta[\phi_{0i}(z)+\epsilon\phi_{1i}(z)\sin ly+\ldots]\exp\mathrm{i}k(x-ct), \quad i = 1,2 \tag{17}$$

exist which satisfy Laplace's equation. It is sufficient for our purposes here to include only terms to order $\delta\epsilon$. Solutions are obtained by matching the pressure and by satisfying the kinematic conditions at the disturbed interface,

$$\eta^* = \delta[\eta_0 + \epsilon\eta_1 \sin ly] \exp ik(x-ct), \tag{18}$$

and by satisfying the Taylor series expansion of the upper and lower boundary conditions. The first-order solution follows that of Drazin & Reid (1981, section 4), giving the eigenvalue equation for the zero-order phase speed, c_0:

$$\rho_1(c_0-U_1)^2 t_2 + \rho_2(c_0-U_2)^2 t_1 = (g/k)\, t_1 t_2(\rho_2-\rho_1), \tag{19}$$

where $t_i = \tanh kH_i$, and the velocity potentials are

$$\phi_{01} = \frac{-i\eta_0}{U_1-c_0}\frac{\cosh k(z-H_1)}{\sinh kH_1}, \quad \phi_{02} = \frac{i\eta_0}{U_2-c_0}\frac{\cosh k(z+H_2)}{\sinh kH_2}. \tag{20}$$

The order-$\delta\epsilon$ interfacial displacement, η_1, is given by

$$\eta_1\left[\frac{gm}{k^2}(\rho_2-\rho_1) - \rho_1\frac{(U_1-c_0)^2}{\tanh mH_1} - \rho_2\frac{(U_2-c_0)^2}{\tanh mH_2}\right] = \eta_0\left[\frac{\rho^2 A_2(U_2-c_0)^2}{\sinh kH_2 \sinh mH_2} - \frac{\rho_1 A_1(U_1-c_0)^2}{\sinh kH_1 \sinh mH_1}\right], \tag{21}$$

where $m = (k^2+l^2)^{1/2}$, which is the z-exponent of the ϕ_{1i} terms.

If, for example, $A_1 = A_2 = A$, $H_1 = -H_2 = H$, and $U_1 = U_2 = 0$ representing a two-layer fluid with no shear, then $c_0^2 = (g\Delta/k)\tanh kH$, where $\Delta = (\rho_2-\rho_1)/(\rho_1+\rho_2)$ is the fractional density difference. Since c_0 is real, the solution is one of propagating waves with a y-modulated amplitude which is equal to $\delta\eta_0[1+(\epsilon Ak^2\Delta/M)\sin ly]$, where $M = m\cosh kH \sinh mH - k\sinh kH\cosh mH$, which is positive.

If however $A_1 = 0$, $A_2 = A$, $H_1 = -H_2 = H$, $\Delta \ll 1$ and $U_1 = -U_2 = U$, representing a shear flow in a channel bounded by a level water surface above and sinusoidal topography below, the phase speed is imaginary, $c_0 = \pm iU(\chi-\chi^{-1})^{1/2}$, $= \pm ic_I$, say, where $\chi = (U^2k/gt\Delta)$ with $t = \tanh kH$, and $\eta_1 = (\eta_0 Ak^2/2M)[1\pm 2i\chi(\chi^2-1)^{1/2}]$. For wavenumbers, k, such that $\chi > 1$, the solution to order $\delta\epsilon$ represents a mode with an exponentially growing component:

$$\begin{aligned}\eta^* &= \delta\eta_0\{1+\epsilon(Ak^2/2M)[1+2i\chi(\chi^2-1)^{1/2}]\sin ly\}\exp(ikx)\exp(c_I t),\\ &= a(y)\exp[i(kx+\phi(y))]\exp(c_I t),\end{aligned} \tag{22}$$

where $a(y) = \delta\eta_0 q$ and $\tan\phi = (\epsilon Ak^2\chi/M)(\chi^2-1)^{1/2}\sin ly$, with

$$q = \{[1+\epsilon(Ak^2/2M)\sin ly].$$

This disturbance has an amplitude, a, which depends on y, and a phase which varies with y, increases with the boundary slope, ϵAk, and increases as the non-dimensional wavenumber, kH, increases for fixed values of lH and $U^2/g\Delta H$.

2.4. *Uniformly sloping boundaries*

In the experiments described in §3 we examine the development of an instability in a stratified shear flow,

$$U = U_0 \operatorname{erf} z/z_0, \quad \text{with} \quad \rho = \rho_0(1-\Delta \operatorname{erf} z/z_0), \tag{23}$$

confined between parallel boundaries at $z = \pm H + \epsilon y\tan\alpha$. The flow is characterized by the minimum Richardson number, $J = g\Delta z_0\pi^{1/2}/(2U_0^2)$ which occurs at $z = 0$, and by the non-dimensional interface thickness scale $\pi^{1/2}z_0/2H$. To a first approximation,

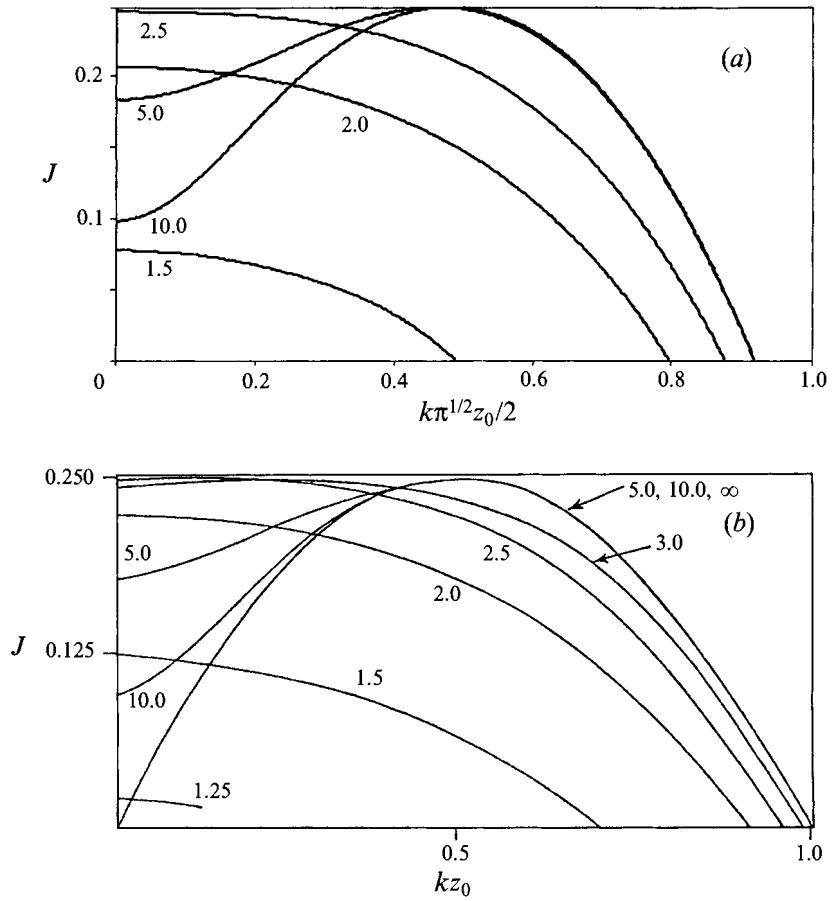

FIGURE 2. The variation of the stability boundaries with boundary separation, for (*a*) the error function profile, (23), at specified values of $2H/\pi^{1/2}z_0$; and (*b*) for $U = U_0 \tanh(z/z_0)$, $\rho = \rho_0[1 - A\tanh(z/z_0)]$ at specified values of H/z_0, reproduced from Hazel (1972).

the lateral boundaries may be taken to be at $y = \pm b$. We write the upper and lower boundary conditions as $z = \pm H + \epsilon \sum a_n \sin l_n y$ with $l_n = \pi(2n+1)/2b$, $n = 0, 1, 2, \ldots$, and $a_n = 8b(-1)^n \tan\alpha/[\pi(2n+1)]^2$. The solution is found as in §2.1 but with

$$w = \delta[w_0 + \epsilon \sum w_{1n} \sin l_n y + \epsilon^2(w_{21} + \sum w_{22n} \cos 2l_n y) + \ldots], \tag{24}$$

where $\mathscr{L}(k, 0)\, w_0 = 0$ with $w_0 = 0$ at $z = H$, giving the eigenvalue equation for c_0, $\mathscr{L}(k, l_n)\, w_{1n} = 0$, with $w_{1n} = -a_n \mathrm{d}w_0/\mathrm{d}z$ at $z = \pm H$. The terms of order $\delta\epsilon^2$ are first w_{21}, which satisfies (7) with

$$w_{21} = \sum \frac{a_n}{2(k^2 + l^2)} \left\{ \frac{a_n l_n^2 U'}{(U - c_0)} \frac{\mathrm{d}w_0}{\mathrm{d}z} - k^2 \frac{\mathrm{d}w_{1n}}{\mathrm{d}z} \right\} \quad \text{at} \quad z = \pm H, \tag{25}$$

so giving an equation for c_2; and secondly w_{22n}, which satisfies $\mathscr{L}(k, 2l_n)\, w_{22n} = 0$ with

$$w_{22n} = \frac{a_n}{2(k^2 + l_n^2)} \left\{ \frac{l_n^2 U' a_n}{(U - c_0)} \frac{\mathrm{d}w_0}{\mathrm{d}z} + (k^2 + 2l_n^2) \frac{\mathrm{d}w_{1n}}{\mathrm{d}z} \right\} \quad \text{at} \quad z = \pm H. \tag{26}$$

The corresponding solution expansion for v (see (5)) satisfies $v = 0$ at the lateral boundaries.

These equations have been solved numerically. Since a_n decreases rapidly with n, a good approximation is found by truncating the series at $n = 4$. The stability of the flow

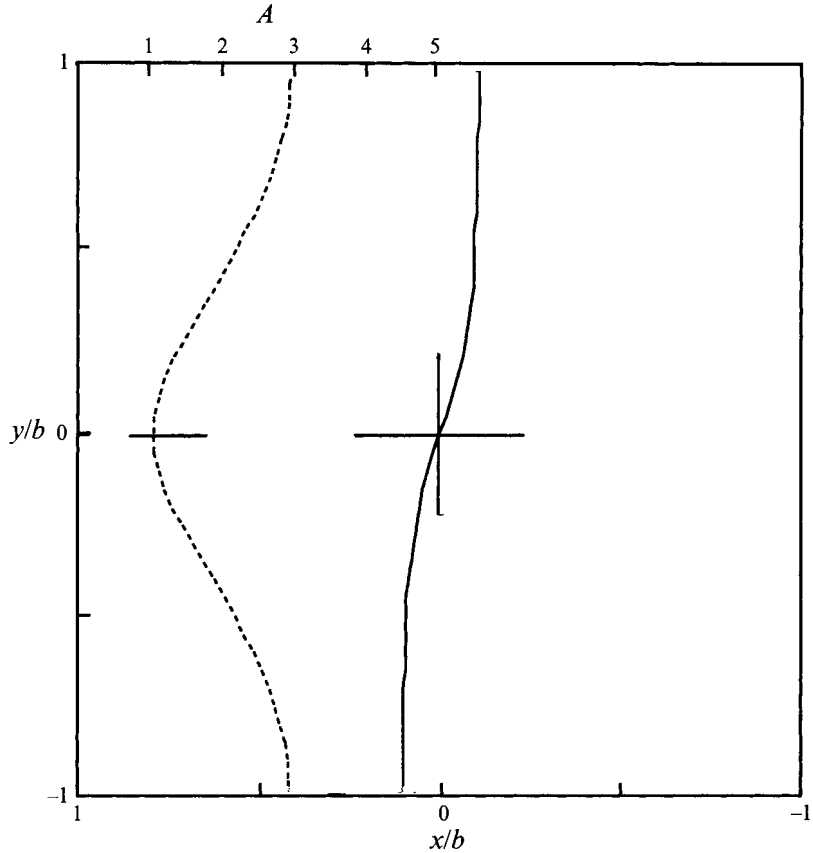

FIGURE 3. The spanwise variation of amplitude (dotted line), $A = 1 + \Sigma w_{1nr} \sin l_n y/w_0$, and the shape of a constant phase line (solid line), with $J = 0.044$, $k = 1.17$ cm^{-1}, $z_0/H = 0.146$, $\alpha = 14.0°$ and the x-axis plotted to increase towards the left, corresponding to the conditions of the experiments shown in figure 7.

(23) in an infinite fluid has been studied by Hazel (1969; see also Thorpe 1971). The critical Richardson number is 0.25 and instability is found at sufficiently small Richardson numbers in a range of non-dimensional wavenumbers, $k\pi^{1/2}z_0/2$, between 0 and 0.91. The effect of plane horizontal boundaries on flows and density profiles of hyperbolic tangent shape, to which the error function profiles, (23), approximate, has been studied by Hazel (1972). He found that as a non-dimensional parameter, H divided by the interface thickness, decreases, the effect is first to destabilize the longer waves and then, as H becomes comparable to the interface thickness, to stabilize the flow. Similar results are found here for the error function profile, as shown in figure 2. The phase speed of the unstable modes is zero.

The variation in the y-direction of the disturbance amplitude and phase of unstable modes may be determined from the expansion to order $\delta\epsilon$, as in §2.3. Since $c_0 = \pm ic_I$ is pure imaginary, and if $w_{1n} = w_{1nr} + iw_{1ni}$, we can write the growing mode of instability as $w^* = W(y,z)\exp(c_I t)\exp i[kx + \phi(y)]$, where

$$W(y,z) = \delta w_0[1 + \epsilon \Sigma w_{1nr} \sin l_n y/w_0] \tag{27}$$

and

$$\tan\phi = \epsilon \Sigma w_{1ni} \sin l_n y/w_0, \tag{28}$$

which is proportional to the boundary slope, $\epsilon \tan\alpha$. The displacement at $z = 0$, where $U = 0$, is then $\eta^* = w^*/kc_I$, so that (27), with division by kc_I, gives the isopycnal

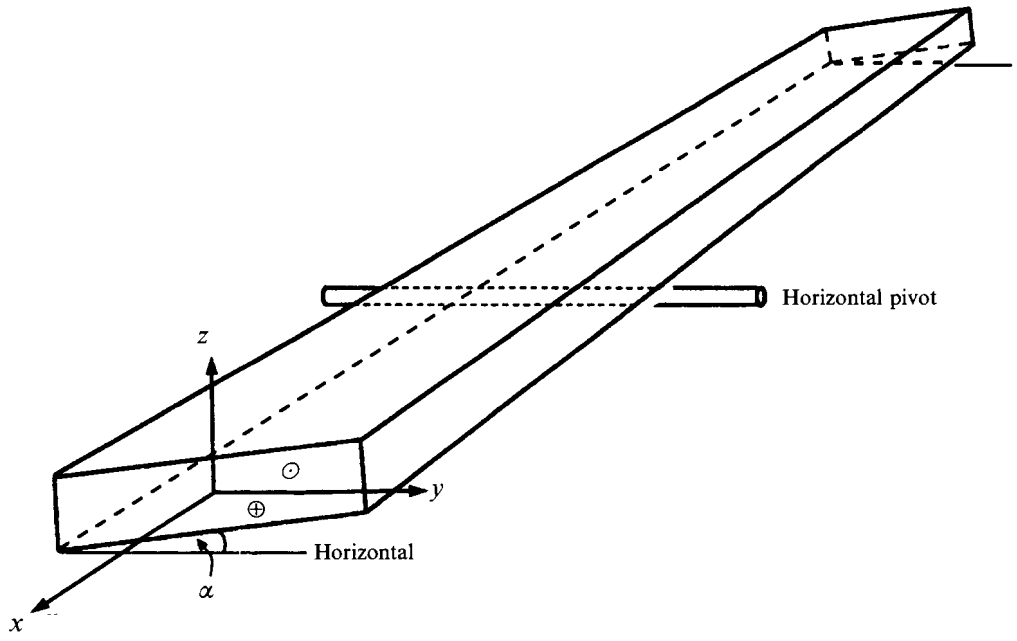

FIGURE 4. Sketch showing the orientation of the tube used in the laboratory experiments, and the coordinate axes.

disturbance amplitude, and (28) gives its variation with phase, as y varies. Figure 3 shows the variation of amplitude and the position of the constant phase line, $kx+\phi(y)$, from $y/b=-1$ to $y/b=1$ for $\alpha=14.0°$, $z_0/H=0.146$, $kH=7.02$ and $J=0.044$. The parameter values and direction of axes are chosen to correspond to a flow realized in the laboratory experiments described in §3. The amplitude is smallest at $y=0$ and the disturbance, the 'crest lines' of growing billows, is twisted across the containing channel. Solving (7), subject to (25), for c_2 with the same parameters gives $c_{2i}/c_0=-2.08\times10^{-3}$ and $c_{2r}=0$, showing that in this case the sloping boundaries have a stabilizing effect. Calculations of c_{2i} in (J,k)-space at the same value of α show that is remains negative, with largest values at small wavenumbers. This shifts the locus of the maximum growth rate (as shown, for example, in Thorpe 1971, figure 2) to larger wavenumbers. This effect contrasts with that of parallel boundaries symmetrically positioned on either side of a density and shear interface, where a reduction in their separation tends to move the fastest growing waves to lower wavenumbers, as illustrated in figure 2. Calculations have also been made with non-symmetrically placed, non-sloping boundaries (i.e. $\alpha=0$, $H_1\neq H_2$). In this case the phase speed, c_{0r}, of the fastest growing mode is no longer zero, but is in the direction of flow in the shallower layer. The critical Richardson number is reduced and the growth rates at given values of k and J are also reduced. These effects are most prevalent on disturbances with large wavenumbers, resulting an increase in the wavelength of the fastest growing disturbances.

3. Experiments

We have made experiments in a Perspex tube 2.45 m in length, with rectangular cross-section 0.2 m × 0.06 m. The tube is filled in the vertical position with two equal layers, the upper being fresh water and the lower a weak brine solution, as described

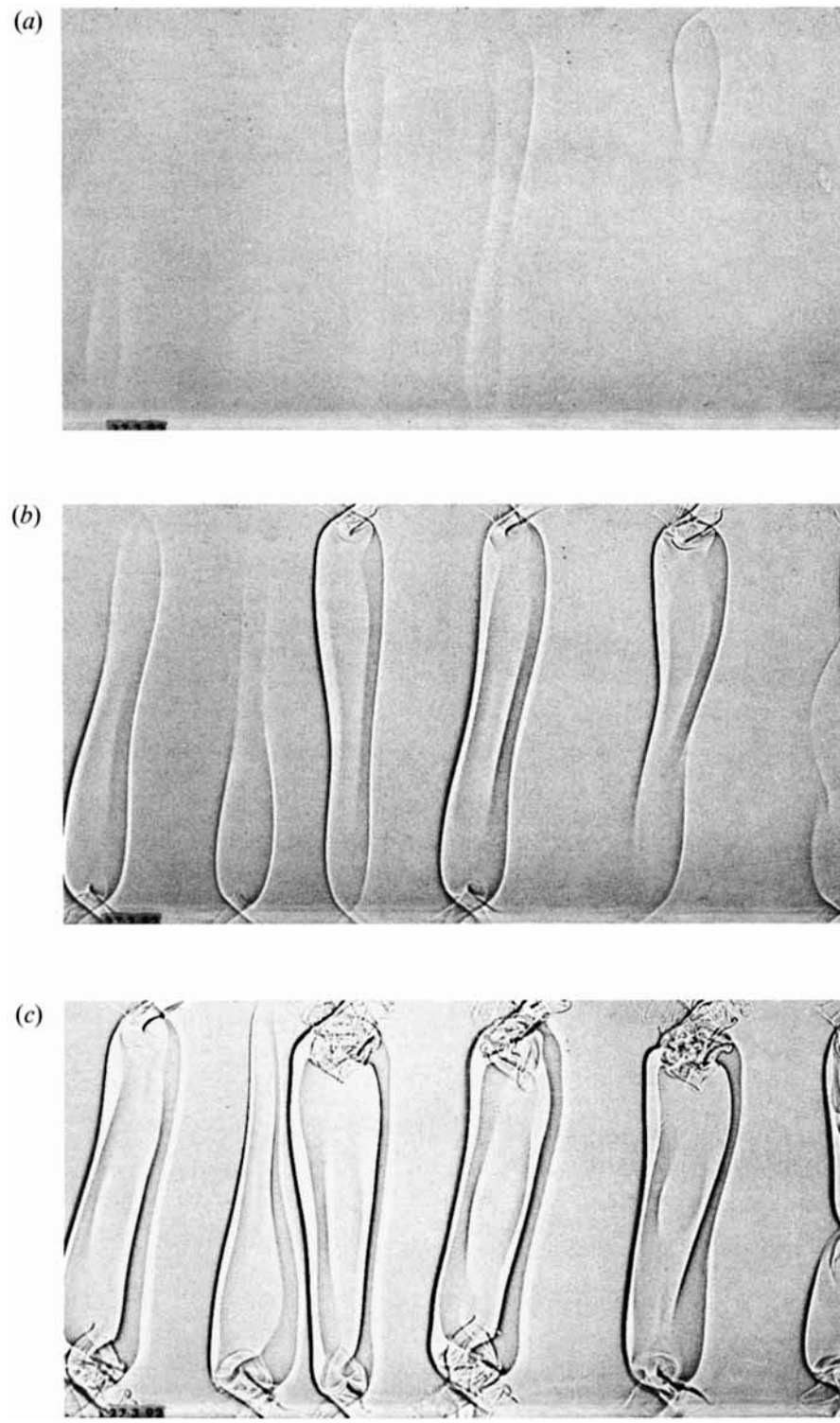

FIGURE 5(*a–c*). For caption see page 59.

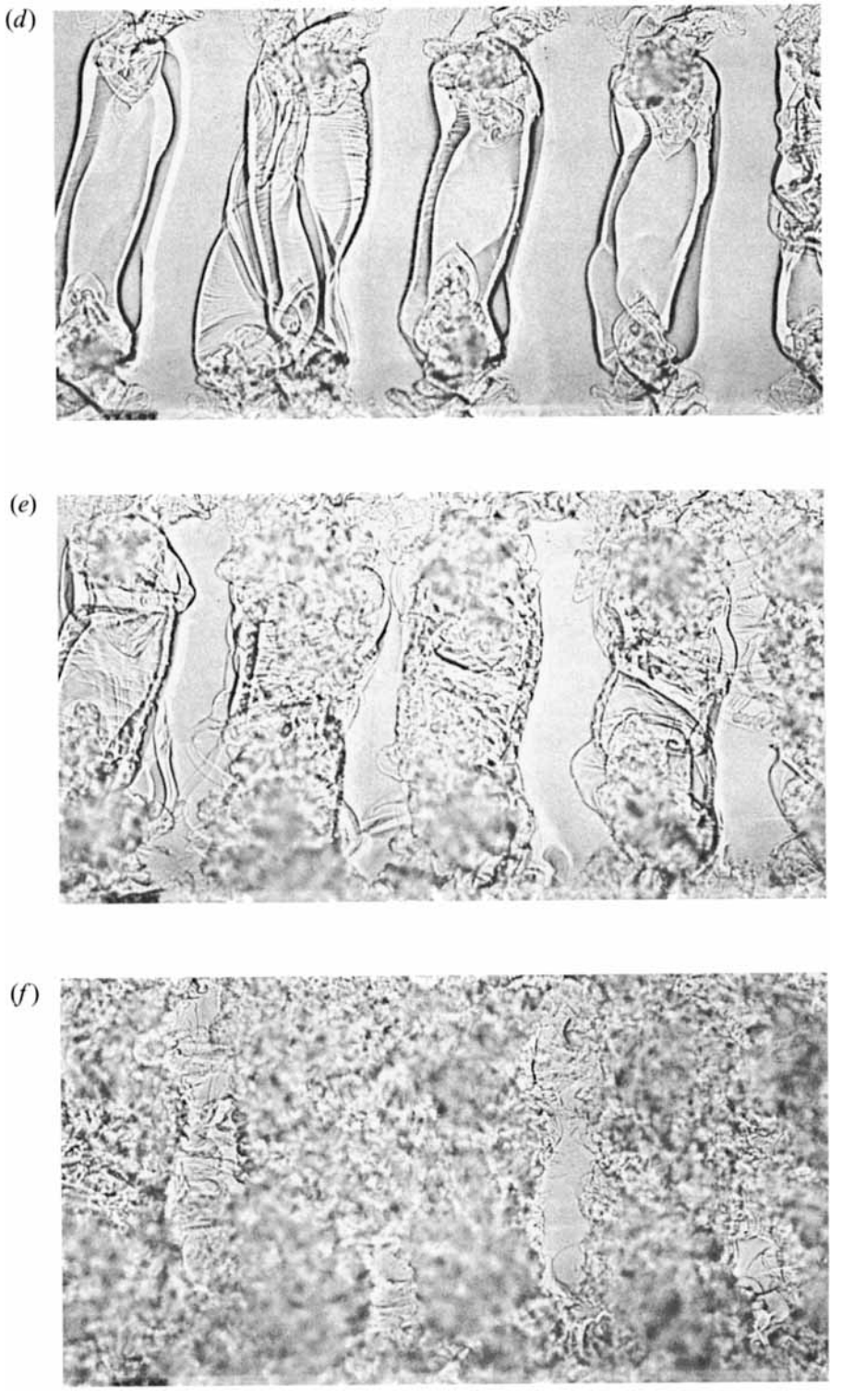

FIGURE 5(*d–f*). For caption see facing page.

by Thorpe (1971). The fractional density difference ranges from 0.029 to 0.041. The tube is then slowly rotated (to avoid much mixing) about a horizontal pivot until the long axis (parallel to the generators) of the tube is horizontal. The pivot is normal to this long axis of the tube but makes an adjustable angle, α, between 3.6 and 15.7° (estimated to within 0.1°) with the 0.2 m long side (as shown in figure 4), so that, after rotation, the lower and upper surfaces of the tube are inclined to the horizontal, and the thicknesses of the fresh water and brine layers vary across the width of the tube. Provided $\alpha < 16.7°$, the centreline of the interface (at $z = 0$) does not intersect the upper and lower surfaces of the tube. Diffusion is then allowed to occur for a time, τ, until the density interface (of approximately error function form) has reached a given thickness, $z_0 = 2[\kappa(\tau+\tau_0)]^{1/2}$, where τ_0 represents a virtual diffusion time associated with filling and tilting the tube to the horizontal. The thickness z_0 is chosen to be between 0.44 and 0.95 cm and estimation to within 0.03 cm. Flow is produced by rapidly tilting the tube about the horizontal pivot through an angle of about 5°. This initiates a uniformly accelerating shear flow (Thorpe 1968) which, except in the viscous boundary layers, is independent of y, has a z-profile similar to the density (i.e. an error function dependence on z), and is maintained until the tube is rapidly returned to the horizontal at a time when the minimum Richardson number has fallen to some value, J, between 0.044 and 0.13 (J is estimated to within ± 0.006). Measurements of velocity from the motion of neutrally buoyant particles when $\alpha = 14.7°$ show that, during the acceleration, the mean spanwise velocity is about 0.2% of the mean flow parallel to the sidewalls; the initial flow is purely longitudinal to well within the experimental uncertainties. The subsequent flow in the centre of the tube is steady, except for viscous effects or the development of instability, until disturbed by the arrival of surges from the ends. Shadowgraphs, taken by shining a beam of light downwards through the tube onto a transparent screen fixed to its lower surface which is photographed by camera or imaged by video from below, and dyed lower layers are used to visualize the development of instability and, in particular, to show the cross-tube shape of the developing billows.

Figure 5 shows shadowgraphs of the development of instability at a Richardson number $J = 0.050$ and tilt angle $\alpha = 6.8°$. The orientation of the flow and other parameters are given in the caption. The billows can be seen to be twisted across the tube, and 'pinched' near the centre of the tube. Figure 6 shows billows at similar states of development and in similar z_0/H and J parameter ranges, but for different tube tilt angles, α. The pinching is enhanced at larger angles, α. Figure 7 shows the development of instability at $\alpha = 14.0°$ and $J = 0.044$. The general form predicted in §2.4 and shown at the same parameter values in figure 3, is reproduced by the first, second and fifth billows from the left in parts (b, c). One 'half-tube wide' billow is seen to develop (at the top, fourth billow from the left), which then connects (figure 7d) to the lower half of both its neighbouring billows. This effect produces a pattern with narrow vortex structures at a large angle to the cross-tube direction. The consequential breakdown of the billow structure (figure 7d–f) contains much more fine structure than is commonly found when the billows are formed more regularly across the tube, as in figure 5(d–f).

FIGURE 5. Shadowgraph taken from below the tube showing the development of instability in a flow with $J = 0.050$, $\alpha = 6.8°$, and $z_0/H = 0.075$. The brine layer decreases in depth from the bottom of the frame to the top and flows to the right. Comparison with figure 4 shows that the corresponding direction of the positive y-axis is upwards and, since the photographs are from beneath the tube, the x-axis is towards the left, as in figure 3. The tube has been tilted (down to the right) for a time $t_0 = 4.50$ s to generate the shear flow, and the times of the photographs are (a) 0.75 s, (b) 1.08 s, (c) 1.40 s, (d) 1.73 s, (e) 2.05 s and (f) 2.38 s after t_0. The imaged region is 19.3 cm in height.

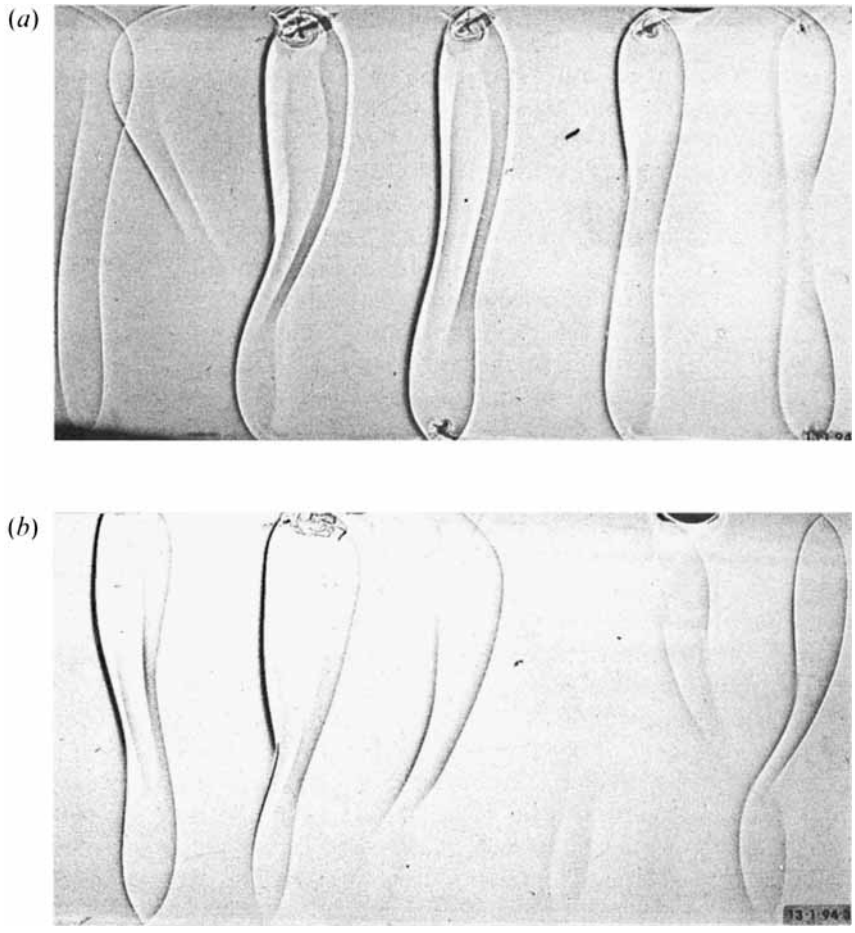

FIGURE 6. Shadowgraphs, as in figure 5, showing the orientation of billows in the tube. (*a*) $J = 0.053$, $z_0/H = 0.154$, $\alpha = 3.8°$, frame width = 19.6 cm and $t_0 = 4.80$ s with the photograph being taken 0.08 s later; (*b*) $J = 0.057$, $z_0/H = 0.154$, $\alpha = 12.7°$, frame width = 18.6 cm and $t_0 = 4.68$ s with the photograph being taken 0.12 s later.

4. Discussion

Although the theory applies strictly to infinitesimal disturbances whilst the images in the shadowgraphs are of well-developed billows, the experiments do exhibit two features predicted by the theory: the reduced amplitude of the disturbances in the centre of the tube and the twisted shape of the billows. The maximum gradient of a line of constant phase occurs at $y = 0$ and is given by $\tan\gamma = -k^{-1}(\mathrm{d}\phi/\mathrm{d}y)$ at $y = 0$, or

$$\tan\gamma = -(\sum l_n w_{1ni})/(kw_{0r}), \tag{29}$$

with values of the w-components evaluated at $z = 0$. A comparison of this predicted value with the experimental observations, calculated using the values of J, kH, z_0/H and α of the experiments, is shown in figure 8. The variation in γ is dominated by variations in k and z_0/H and through the scaling of w_{1n}, (29), $\tan\gamma$ is proportional to $\tan\alpha$. The values of γ are relatively insensitive to changes in J. Some agreement is found when the predicted γ is small; the r.m.s. deviation of the observed angle from that predicted is 6.5° for $0 < \gamma < 40°$. Above 40°, (29) overpredicts the mean 'twist'

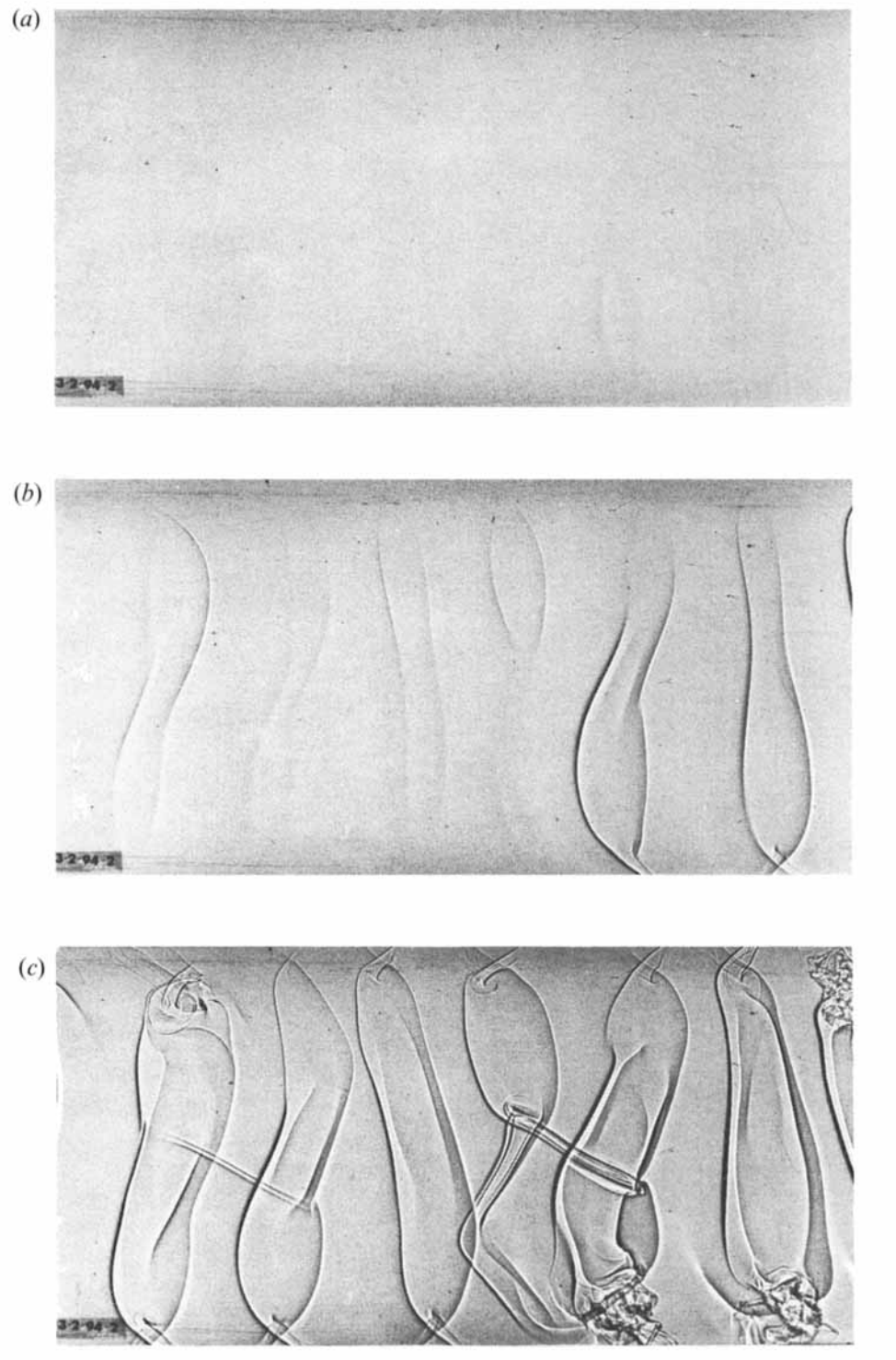

FIGURE 7(*a–c*). For caption see page 63.

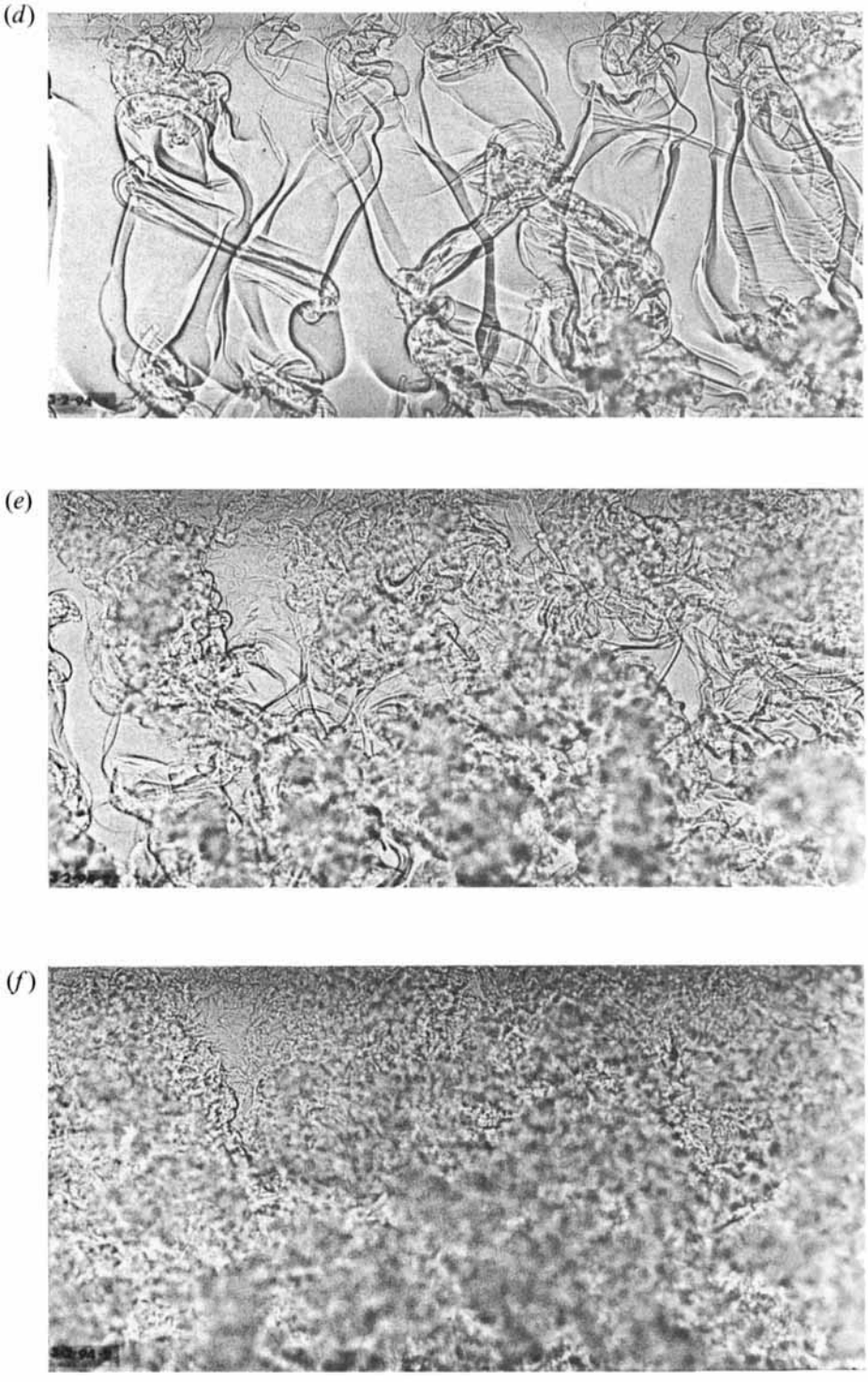

FIGURE 7(*d–f*). For caption see facing page.

angle. These points generally correspond to large $\alpha (> 11°)$ or to values of $2H/\pi^{1/2}z_0$ which are less than 10, the value (Hazel, 1972) at which the presence of boundaries has an appreciable effect on the development of the instability. In these conditions w_{1ni} is of similar magnitude to w_{0r}, and the truncation of the series expansion for w at order $\delta\epsilon$ is no longer valid. In the experiments a qualitative change in the appearance of the billow structure occurs. There is no longer a clear spanwise variation in the billow angle, but the billows evolve as alternating large negatively sloping and small positively sloping billows connected close to the sidewalls to form a wall-to-wall zigzag structure.

Individual billows observed in past experiments on stratified shear flows confined between parallel horizontal boundaries are often observed to be slightly tilted across the containing tube. Examples can be seen in Thorpe (1971, figure 5; 1985, figure 6; and 1987, figure 4). In consequence, very rarely in a subsequent 'pairing' of neighbouring billows a precisely two-dimensional process. On average however the billow orientation is transverse to the mean flow, i.e. the mean lines of constant phase are parallel to the mean flow vorticity. It is hardly surprising that the orientations of the billows seen, for example in figures 5 and 7, are not all parallel or tilted in exactly the same directions across the tube. Some variation, evident in the scatter bars of figure 8, is a result.

It is assumed, in making comparison with the theoretical results of §2.4, that the presence of the non-vertical sidewalls does not affect the onset and small-amplitude growth of the instability in the body of the tube, and that the effects of the viscous boundary layers which occur at the sidewalls (and at the upper and lower boundaries) of the tube, are negligible. It is clear in the photographs, however, that the sidewalls introduce substantial local changes in the form of the billows, 'pinching' them and producing a crossing structure in the shadowgraph images within about 1 cm of the walls (e.g. see top of figure 5*b*). An early transition to turbulence is triggered in their vicinity (figure 5*c*). These effects are also apparent in experiments with horizontal upper and lower boundaries (Thorpe 1985, figure 6*a–d*; and 1987, figure 4) when turbulence also sets in at an earlier stage near the sidewalls than in the centre of the tube; the billows seen here are not significantly different. It is worth asking whether the *tilt* of the sidewalls may produce novel effects. A full consideration would require at least the development of solutions which satisfy the condition of no flow normal to the tilted sidewalls, and this is not attempted. We have however considered one effect, that of increasing the across-tube length of the density interface. The maximum possible increase is from $2b$ to $2(b^2+H^2)^{1/2}$ when $\alpha = \tan^{-1}(H/b)$, so that the interface length is increased from 20 to 20.9 cm, and this results in an increase in the modulus of the estimated 'twist' angle of 4.6% when $\gamma = 54.2°$ and of 4.9% when $\gamma = 33.2°$. This effect is small in comparison to the existing uncertainties of prediction indicated in figure 8. The thickness of the viscous boundary layers at the sidewalls at the time of onset of instability (typically 5–6 s) will also have an effect, reducing the transverse width of the interface over which there is a shear by some 0.8 cm and tending to mask the effects of sidewall tilt. Two other factors may affect transitional phenomena. For large angles of tilt, α, one fluid layer near the sidewalls is shallow, and interfacial waves derived from disturbances when the tube is tilted, and propagating across the tube into a shallowing layer, may be amplified, as are waves approaching a beach. More important is that if

FIGURE 7. Shadowgraph, as in figure 5, showing the development of billows when $J = 0.044$, $z_0/H = 0.146$, $\alpha = 14.0°$. The tube is tilted for a time $t_0 = 4.40$ s and the times of the photographs are (*a*) 0.50 s, (*b*) 0.82 s, (*c*) 1.14 s, (*d*) 1.50 s, (*e*) 1.86 s and (*f*) 2.20 s after t_0. The imaged region is 18.5 s wide. The focal plane of the camera is horizontal, leading to some perspective distortion, about 3° at the frame edge.

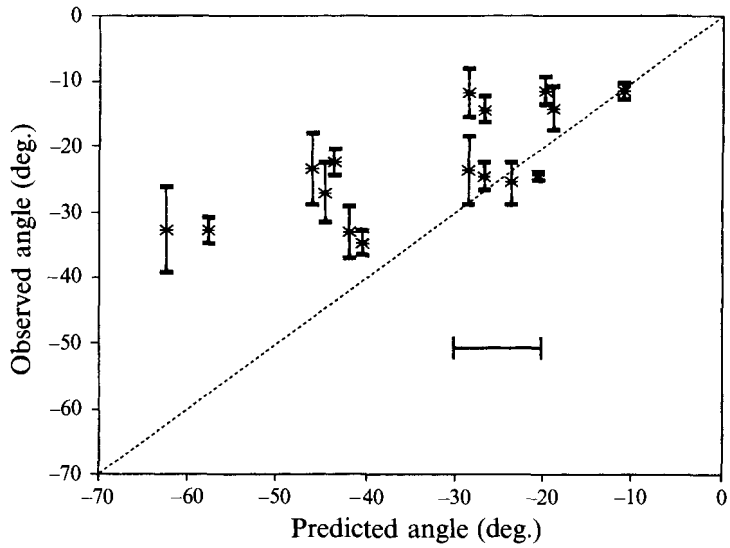

FIGURE 8. Comparison of estimated and observed 'twist' angle of the billows at $y = 0$. Data are taken from 16 experiments with $0.044 < J < 0.114$ and $0.39 < k\pi^{1/2}z_0/2 < 0.59$. The vertical error bars represent the standard deviation from the mean of the observed billow angles, and the horizontal bar represents the typical uncertainty resulting from probable errors in the experimental values in estimating the billow angle from (29).

the developing billow vortices are not normal to the sidewalls, the vortices may be severely distorted locally by the flow field arising from their effective image system.

Whilst the nature of the transition to turbulence is beyond the scope of this paper, comparison of figures 5 and 7 shows that the more severe the amplitude and phase distortion of the billows, the more frequent is the subsequent occurrence of 'knots' and connecting 'vortex tubes' described by Thorpe (1985, 1987). It is not known if, or when, the fine structure and enhanced turbulent diffusion of mass and momentum associated with these features dominates over that resulting from the winding-up and subsequent secondary instability of isopycnal surfaces in the billows. The presence of such regions of turbulence does however suggest a novel mechanism by which topography may locally enhance clear-air turbulence in the atmosphere. A particular application of the results is to the development of instability in stratified estuaries, channels or shallow lakes. It is expected that billows developing in the ocean or the atmosphere on a shear layer lying between, or adjacent to, stable layers of large density gradient on which internal waves are propagating, will also be distorted by their presence. This may explain why the linear billow clouds (Ludlam 1987) seen, for example, in altocumulus layers in the atmosphere preceding warm fronts, are often non-parallel.

J.T.H. was supported by a studentship from the Natural Environment Research Council, and his contribution to this paper forms part of a PhD dissertation submitted to the University of Southampton.

REFERENCES

BANKS, W. H. H., DRAZIN, P. G. & ZATURSKA, M. B. 1976 On the normal modes of parallel flow of inviscid stratified fluid. *J. Fluid Mech.* **75**, 149–171.

DRAZIN, P. G. & REID, W. H. 1981 *Hydrodynamic Stability*. Cambridge University Press.

GRIMSHAW, R. 1978 Long non-linear internal waves in channels of arbitrary cross-section. *J. Fluid Mech.* **86**, 415–431.

HAZEL, P. 1969 Numerical studies of stratified shear flows. PhD thesis, University of Cambridge.

HAZEL, P. 1972 Numerical studies of the stability of inviscid stratified shear flows. *J. Fluid Mech.* **51**, 39–61.

LUDLAM, F. H. 1967 Characteristics of billow clouds and their relation to clear-air turbulence. *Q. J. R. Met. Soc.* **93**, 419–435.

THORPE, S. A. 1968 A method of producing a shear flow in a stratified fluid. *J. Fluid Mech.* **32**, 693–704.

THORPE, S. A. 1971 Experiments on the stability of stratified shear flow: miscible fluids. *J. Fluid Mech.* **46**, 299–319.

THORPE, S. A. 1978 On the shape and breaking of finite amplitude internal gravity waves in a shear flow. *J. Fluid Mech.* **85**, 7–31.

THORPE, S. A. 1985 Laboratory observations of secondary structures in Kelvin–Helmholtz billows and consequences for ocean mixing. *Geophys. Astrophys. Fluid Dyn.* **34**, 175–199.

THORPE, S. A. 1987 Transitional phenomena and the development of turbulence in stratified fluids; a review. *J. Geophys. Res.* **92**, 5231–5248.

YIH, C. S. 1955 Stability of two-dimensional parallel flows for three dimensional disturbances. *Q. Appl. Maths* **12**, 434–435.